A Comparative Ab Initio and DFT Study of Polyaniline Leucoemeraldine Base and Its Oligomers

ARTICLE *in* THE JOURNAL OF PHYSICAL CHEMISTRY B · NOVEMBER 2009

Impact Factor: 3.3 · DOI: 10.1021/jp906799m · Source: PubMed

2 AUTHORS:

Abhishek KUMAR Mishra
University College London
20 PUBLICATIONS **138** CITATIONS
SEE PROFILE

Poonam Tandon
University of Lucknow
206 PUBLICATIONS **989** CITATIONS
SEE PROFILE

A Comparative *Ab Initio* and DFT Study of Polyaniline Leucoemeraldine Base and Its Oligomers

Abhishek Kumar Mishra* and Poonam Tandon

Department of Physics, University of Lucknow, Lucknow-226 007, India

Received: July 18, 2009; Revised Manuscript Received: September 7, 2009

Ab initio Hartree−Fock (HF) and density functional theory (DFT) calculations are being performed to investigate the geometric, vibrational, and electronic properties of the polyaniline leucoemeraldine base (PANI-LB). Vibrational spectra of PANI-LB have been analyzed using the DFT oligomer approach, and complete assignments are being reported. Lower region spectral assignments of the PANI-LB which were not being reported earlier are being done in the present work. DFT calculations with the 6-31G** basis set produce very good results of not only vibrational modes but also of energy band gap.

1. Introduction

Since the discovery of metal-like electrical conductivity in polyacetylene,[1] there have been various studies on the physical and chemical properties of conjugated electroactive polymers.[2] Among them, members of polyaniline (PANI) have received considerable attention due to the controllable electrical conductivity,[3] environmental stability,[4] and interesting redox properties associated with the chain hetroatoms.[5]

PANI, a green intractable powder, has a history beginning more than 140 years ago, when in 1862 Letheby[6] reported on the electrochemical oxidation product of aniline and in 1968 Surville et al.[7] on the high electrical conductivity and its pure electronic character in PANI, which depends on the "acidity, redox level & hydration"[7] of the polymer. PANI was rediscovered a few years ago as a very important member of conducting polymers having wide potential technological applications.[8−13] It is also used as an electrode material for semiconductor batteries,[11,14−18] as a semiconducting material,[19] as a sensor material,[20] as an electrochromic-display material,[21−23] and as a catalyst for photoelectrochemical processes.[23]

PANI relates to a large class of polymers, as several forms of these compounds can be obtained. These different forms are described by two parameters: the average oxidation state[24,25] and the degree of protonation.[26,27] These conducting polymers differ substantially from polyacetylene and other aromatic and hetroaromatic polymers in the fact that their electronic structure is based on the overlap of alternating nitrogen and C6 rings. In its nonconductive undoped (or base) form, PANIs have the general formula $[(-B-NH-B-NH-)_y(-B-N=Q=N-)_{1-y}]_x$ (B and Q stands for benzoid and quinoid structure, respectively), where y can be varied continuously from 1 to 0 (from the completely reduced form to the completely oxidized one). The conversion to a conductive form can be accomplished by either protonic or electronic doping.[28,29] The terms leucoemeraldine, emeraldine, and pernigraniline refer to the different oxidation states of the polymer where $y = 1$, ~0.5, and 0, respectively. In this work, we have focused all of our attention on the fully reduced ($y = 1$) non-protonated form (leucoemeraldine base: LB).

* Corresponding author. Phone: +91-522-2648064. E-mail: drabhishekkmishra@yahoo.in.

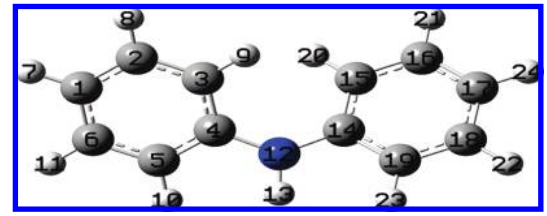

Figure 1. B3LYP/6-31G** optimized geometry of DPA.

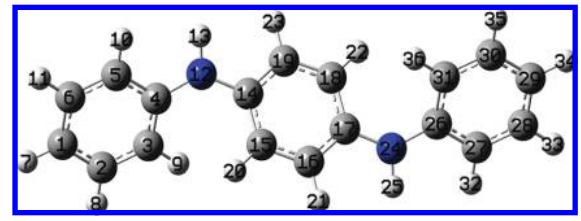

Figure 2. B3LYP/6-31G** optimized geometry of PCD (B3).

TABLE 1: Optimized Geometry of DPA, Calculated Using *Ab Initio* HF and DFT Methods (Atomic Labels Are with Reference to Figure 1)

geometrical parameters	HF/6-31G**	B3LYP/ 6-31G**	experimental[30]
	Bond Length (Å)		
N12−C4, N12−C14	1.400, 1.399	1.399, 1.399	1.401, 1.406
C4−C3, C14−C15	1.391, 1.394	1.406, 1.406	
C3−C2, C15−C16	1.386, 1.383	1.394, 1.394	
C2−C1, C16−C17	1.383, 1.386	1.395, 1.395	
C1−C6, C17−C18	1.386, 1.384	1.396, 1.396	
C6−C5, C18−C19	1.381, 1.384	1.391, 1.391	
C5−C4, C19−C14	1.395, 1.391	1.407, 1.407	
	Bond Angle (deg)		
C4−N12−C14	127.0	129.8	124.5
N12−C4−C3	123.3	123.1	
N12−C14−C15	121.5	123.1	
	Dihedral Angle (deg)		
C14−N12−C4−C3	15.9	24.9	23.0
C4−N12−C14−C15	46.2	24.7	36.9

Since the electronic properties of the compounds are directly associated to the chemical bonding and the electron distribution along the polymer backbone, a clear knowledge of their vibrational properties can be of major importance. Vibrational

10.1021/jp906799m CCC: $40.75
Published on Web 10/14/2009

TABLE 2: Optimized Geometry of PCD, Calculated Using *Ab Initio* HF and DFT Methods (Atomic Labels Are with Reference to Figure 2)

geometrical parameters	HF/6-31G**	B3LYP/ 6-31G**	experimental[30]
	Bond Length (Å)		
N12−C4, N12−C14	1.400, 1.406	1.396, 1.403	1.399, 1.416
C4−C3, C14−C15	1.391, 1.390	1.407, 1.405	
C3−C2, C15−C16	1.386, 1.383	1.394, 1.391	
C2−C1, C16−C17	1.383, 1.389	1.395, 1.404	
C1−C6, C17−C18	1.387, 1.388	1.397, 1.405	
C6−C5, C18−C19	1.380, 1.383	1.391, 1.391	
C5−C4, C19−C14	1.396, 1.390	1.408, 1.404	
	Bond Angle (deg)		
C4−N12−C14	125.7	129.2	128.9
N12−C4−C3	123.4	123.1	
N12−C14−C15	121.1	122.9	
	Dihedral Angle (deg)		
C14−N12−C4−C3	5.8	18.3	20.0
C4−N12−C14−C15	58.9	33.5	16.0

TABLE 3: Optimized Geometry of B5, Calculated Using *Ab Initio* HF and DFT Methods (Atomic Labels Are with Reference to Figure 3)

geometric parameters	HF/6-31G**	B3LYP/6-31G**
	Bond Length (Å)	
N12−C4, N12−C14	1.394, 1.425	1.395, 1.405
C1−C2, C16−C17	1.384, 1.397	1.395, 1.406
C1−C6, C17−C18	1.386, 1.392	1.397, 1.405
C2−C3, C15−C16	1.384, 1.379	1.394, 1.400
C3−C4, C14−C15	1.393, 1.390	1.407, 1.405
C4−C5, C14−C19	1.396, 1.384	1.408, 1.403
C5−C6, C18−C19	1.381, 1.385	1.391, 1.391
	Bond Angle (deg)	
C4−N12−C14	122.6	129.0
N12−C4−C3	122.2	123.1
N12−C14−C15	119.9	122.8
	Dihedral Angle (deg)	
C14−N12−C4−C3	22.2	16.0
C4−N12−C14−C15	72.6	36.2

spectroscopy has the potential to yield valuable structural and conformational information on polymers, if used in conjunction with accurate quantum chemical vibrational calculations. A lot of studies have therefore been carried out on this unusual class of conducting polymers to investigate their vibrational properties.[30−36] Various theoretical investigations of conjugated organic molecules and polymers have demonstrated the importance of electron correlation effects. The traditional method of accurately calculating the electronic properties of a molecule is to first perform a Hartree−Fock (HF) calculation followed by a subsequent computation of electron correlation effects using the many-body perturbation theories[37,38] or the coupled-cluster

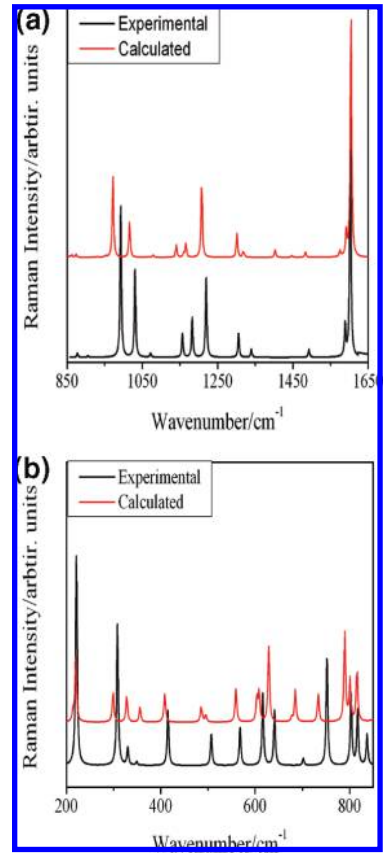

Figure 4. (a) Experimental[32] and calculated Raman spectra of DPA (850−1650 cm^{-1}). (b) Experimental[35] and calculated Raman spectra of DPA (200−850 cm^{-1}).

methods.[39,40] Alternatively, density functional theory (DFT) has provided another way of estimating the correlation effects at a lower computational cost. In fact, DFT has currently received a great deal of attention in the determination of ground state properties of small and medium size molecules[41−44] and infinite polymer systems[45−50] as well. Systematic comparisons between DFT and many-body methods have demonstrated that molecular properties such as geometry, electronic, and band structures can be reliably and significantly obtained from DFT methods.

In continuation to our recent work on PANI,[50] in the present work, we have determined the geometric, vibrational, and electronic properties of leucoemeraldine base polyaniline (PANI-LB) by performing *ab initio* and DFT quantum chemical calculations on its different oligomers, that are also known as model compounds and are namely diphenyl amine (DPA), phenyl-end-capped dimer (PCD or B3), and phenyl-end-capped tetramer (B5). Predictions of the theoretical methods are discussed and compared with each other, and the role ofelectron correlation in the DFT approach is also discussed. It is not possible to calculate vibrational frequencies of an infinite PANI

Figure 3. B3LYP/6-31G** optimized geometry of B5.

TABLE 4: Observed and Calculated Raman and IR Frequencies of DPA (in cm^{-1})[a]

observed frequency			
Raman	IR	calculated frequency	assignments (% PED)
1603		1604	R1[υ(CC)(28) + δ(CCC)(5)] + R2[υ(CC)(28) + δ(CCC)(5)] (*8a*)
1589	1596	1592	R1[υ(CC)(29) + δ(CCC)(5)] + R2[υ(CC)(29) + δ(CCC)(5)] (*8a*)
	1581	1581	R1[υ(CC)(29)] + R2[υ(CC)(29)] (*8b*)
1589		1575	R1[υ(CC)(35)] + R2[υ(CC)(35)] (*8b*)
	1518	1504	R1[δ(CHC)(9) + υ(CC)(5)] + R2[δ(CHC)(9) + υ(CC)(5)] + δ(CHN)(27) + υ(CN)(11) oop(HCCC)(5) + υ(NC)(11) (*19a*)
1493		1483	R1[δ(CHC)(28) + υ(CC)(17)] + R2[δ(CHC)(29) + υ(CC)(17)] (*19b*)
	1494	1478	R1[δ(CHC)(22) + υ(CC)(11)] + R2[δ(CHC)(22) + υ(CC)(11)] (*19a*)
		1448	R1[δ(CHC)(25) + υ(CC)(16)] + R2[δ(CHC)(25) + υ(CC)(17)] + δ(CNC)(6) (*19b*)
	1417	1403	R1[δ(CHC)(21) + υ(CC)(13)] + R2[δ(CHC)(21) + υ(CC)(13)] + δ(CHN)(17)
1340	1336	1321	R1[δ(CHC)(8) + υ(CC)(29)] + R2[δ(CHC)(8) + υ(CC)(29)] + υ(CN)(12) (*3*)
	1318	1318	R1[δ(CHC)(27) + υ(CC)(13)] + R2[δ(CHC)(27) + υ(CC)(13)] (*3*)
1306		1302	R1[δ(CHC)(7)] + υ(CC)(34)] + R2[δ(CHC)(7) + υ(CC)(34)] (*14*)
		1300	R1[δ(CHC)(25)] + R2[δ(CHC)(25)] + υ(CN)(14) + υ(NC)(14)
	1248	1229	R1[υ(CC)(22) + δ(CHC)(7)] + R2[υ(CC)(22) + δ(CHC)(7)] + δ(CHN)(14)
1220		1208	R1[υ(CC)(10)] + R2[υ(CC)(10)] + υ(CN)(20) + υ(NC)(20)
1183	1172	1166	R1[δ(CHC)(40) + υ(CC)(4)] + R2[δ(CHC)(40) + υ(CC)(4)] (*9a*)
1157	1151	1160	R1[δ(CHC)(39) + υ(CC)(3)] + R2[δ(CHC)(39) + υ(CC)(3)] (*15*)
		1140	R1[δ(CHC)(39) + υ(CC)(3)] + R2[δ(CHC)(39) + υ(CC)(3)]
		1140	R1[δ(CHC)(38) + υ(CC)(6)] + R2[δ(CHC)(37) + υ(CC)(3)]
1072	1084	1078	R1[δ(CHC)(20) + υ(CC)(22)] + R2[δ(CHC)(20) + υ(CC)(22)] (*18b*)
		1066	R1[δ(CHC)(18) + υ(CC)(25)] + R2[δ(CHC)(18) + υ(CC)(25)]
1031		1017	R1[δ(CHC)(3) + υ(CC)(31)] + R2[δ(CHC)(3) + υ(CC)(31)] (*18a*)
	1022	1016	R1[δ(CHC)(8) + υ(CC)(31)] + R2[δ(CHC)(7) + υ(CC)(29)] (*18a*)
993		972	R1[δ(CCC)(33) + υ(CC)(10)] + R2[δ(CCC)(33) + υ(CC)(10)] (*12*)
	991	971	R1[δ(CCC)(36) + υ(CC)(8)] + R2[δ(CCC)(36) + υ(CC)(8)] (*12*)
		953	R1[oop(HCCC)(41)] + R2[oop(HCCC)(41)]
		946	R1[oop(HCCC)(41)] + R2[oop(HCCC)(41)]
		929	R1[oop(HCCC)(45)] + R2[oop(HCCC)(44)]
		923	R1[oop(HCCC)(45)] + R2[oop(HCCC)(45)]
878	878	874	R1[oop(HCCC)(39)] + R2[oop(HCCC)(39)]
		863	R1[δ(CCC)(11) + υ(CC)(18)] + R2[δ(CCC)(11) + υ(CC)(18)]
	846	857	R1[oop(HCCC)(39)] + R2[oop(HCCC)(39)]
837		816	R1[oop(HCCC)(41)] + R2[oop(HCCC)(41)]
818		801	R1[oop(HCCC)(49)] + R2[oop(HCCC)(49)]
803		790	R1[δ(CCC)(8) + oop(HCCC)(5) + υ(CC)(8)] + R2[δ(CCC)(8) + oop(HCCC)(5) + υ(CC)(8)] + δ(CCN)(16) + oop(NCCC)(6) + υ(CN)(10)
752		734	R1[oop(HCCC)(26) + τ(CCCC)(9)] + R2[oop(HCCC)(26) + τ(CCCC)(9)] + oop(NCCC)(12)
	745	732	R1[oop(HCCC)(22) + τ(CCCC)(13)] + R2[oop(HCCC)(22) + τ(CCCC)(13)] + oop(NCCC)(18)
702		685	R1[oop(HCCC)(11) + τ(CCCC)(33)] + R2[oop(HCCC)(11) + τ(CCCC)(31)] + oop(NCCC)(10)
	688	677	R1[oop(HCCC)(12) + τ(CCCC)(33)] + R2[oop(HCCC)(12) + τ(CCCC)(33)] + oop(NCCC)(9)
641	641	629	R1[δ(CCC)(20)] + R2[δ(CCC)(20)] + δ(CCN)(13) + δ(CNC)(12)
616	613	608	R1[δ(CCC)(40)] + R2[δ(CCC)(40)]
		603	R1[δ(CCC)(35) + τ(CCCC)(4)] + R2[δ(CCC)(35) + τ(CCCC)(4)] + δ(CCN)(11)
568	568	559	R1[δ(CCC)(43)] + R2[δ(CCC)(43)]
507	505	495	R1[τ(CCCC)(20)] + R2[τ(CCCC)(20)] + oop(NCCC)(40)
		486	R1[τ(CCCC)(21)] + R2[τ(CCCC)(21)] + oop(NCCC)(32)
415	428	408	R1[τ(CCCC)(40)] + R2[τ(CCCC)(39)]
		402	R1[τ(CCCC)(41)] + R2[τ(CCCC)(41)]
		356	oop(HCCN)(20) + τ(CCNH)(35) + τ(CNCC)(35)
		328	R1[τ(CCCC)(6)] + R2[τ(CCCC)(6)] + δ(CNC)(60)
308		299	R1[δ(CCC)(15)] + R2[δ(CCC)(15)] + δ(CCN)(6) + δ(CNC)(18) + υ(CN)(14) + υ(NC)(14)
221		220	R1[oop(HCCC)(9) + τ(CCCC)(29)] + R2[oop(HCCC)(9) + τ(CCCC)(28)] + δ(CCN)(6) + δ(CNC)(6)
		214	R1[τ(CCCC)(28)] + R2[τ(CCCC(28)] + δ(CNC)(8) + oop(NCCC)(8) + τ(CCNH)(6) + τ(CNCC)(6)
		105	R1[τ(CCCC)(20)] + R2[τ(CCCC)(20)] + δ(CCN)(21) + δ(CNC)(10)
		53	δ(CCN)(26) + δ(CNC)(18) + τ(CCNH)(25) + τ(CNCC)(25)
		34	oop(HCCN)(28) + τ(CCNH)(32) + τ(CNCC)(32)

[a] Note: All frequencies are in cm^{-1}. The numbers in italics in parentheses are benzene Wilson numbers. R1 and R2 are the two benzoid rings, and N1 and N2 are the two nitrogen atoms in the molecular structure of DPA. υ, δ, and τ are the symbols used for stretch, bend, and torsional motions. oop: out-of-plane.

chain by using the DFT method at present. Computational methods that are currently used to derive the vibrational force fields of polymers can be classified mainly in two categories: the polymer approach and the oligomer approach. In the polymer approach, the force constants of infinite polymers are directly evaluated by the crystal orbital method, and in the oligomer approach, the force constants of oligomers, which are usually calculated by the *ab initio* molecular orbital or density functional methods, are transferred to polymers. In the oligomer approach, generally the force constants of oligomers cannot be directly

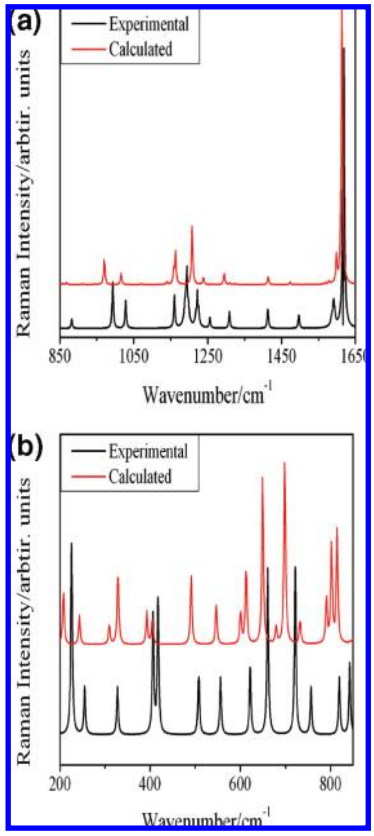

Figure 5. (a) Experimental[32] and calculated Raman spectra of PCD (850−1650 cm^{-1}). (b) Experimental[35] and calculated Raman spectra of PCD (200−850 cm^{-1}).

transferred to polymers because the force constants of oligomers depend strongly on their chain lengths, and due to slow convergence of the force constants as a function of chain length, there is a need for extrapolation of force constants of the infinite chains by approximating the chain-length dependence of the force constants by some phenomenological functions. Although the phenomenological functions may possess information about the force constants of oligomers with intermediate chain lengths, the arbitrariness of these functions cannot be completely removed. In the present work, we have made the normal coordinate calculations of a long oligomer having five phenyl rings and assigned the observed infrared (IR) and Raman spectra[32,35] of PANI-LB by selecting the bands from B5 corresponding to the optically active vibrations of PANI-LB on the basis of the Raman and IR intensities and atomic displacements of vibrational modes. This approach of interpretation of vibrational spectra of polymers has already been used by many workers on different polymers.[51−53] Present work has been performed using both HF and DFT approaches with a higher basis set (6-31G**). DFT with the 6-31G** basis set not only produces quite accurate values of geometrical parameters of the oligomers but also gives us the good fit with the observed spectra.[32,35]

2. Methodology

The *ab initio* and DFT calculations are being performed with the Gaussian 03 program[54] and are analyzed with the help of the GaussView[55] and Chemcraft programs.[56] The geometries of the oligomers are fully optimized, i.e., without any physical constraint or forced symmetry using the 6-31G** split-valence basis set, at the *ab initio* HF and DFT levels. We have adopted the common notation of, say, HF/6-31G** to denote a HF calculation with the 6-31G** basis set. The DFT calculations were mainly carried out in the framework of the Becke−Lee−Yang−Parr (B3LYP) functionals, in which the exchange functional is a local spin density exchange with Becke gradient correction[57] and the correlation functional is that of Lee, Yang, and Parr with both local and nonlocal terms.[58]

The absolute Raman scattering and IR absorption intensities are calculated in the harmonic approximation at the same level of theory as that used for the optimized geometries. The normal-mode analysis is being performed, and the potential energy distribution (PED) is calculated along the internal coordinates using localized symmetry.[59,60] As we know that HF calculations tend to overestimate the frequencies of different modes, and this tendency cannot be eliminated by the standard scaling procedures,[61,62] the situation can be improved if we include DFT because density functional calculations can include electron correlation with modest computational cost. The vibrational frequencies calculated with appropriate functionals are often in good agreement with the observed frequencies when the calculated frequencies are uniformly scaled with only one scaling factor.[63,64] In the present work, all of the calculated frequencies are scaled with a common scaling factor of 0.9613. The vibrational assignments of the normal modes are being done on the basis of the band profile, intensity, and PED, calculated using the GAR2PED program.[65]

In this work, assuming the simplified single configuration electronic transition picture based on Koopman's theorem, the energy band gap is taken as the energy difference between the lowest unoccupied (LUMO) and the highest occupied (HOMO) molecular orbitals of the optimized geometry.

3. Results and Discussion

The molecular structures of the three oligomers, viz., DPA, PCD (B3), and B5, are being discussed in this section followed by the discussion of the vibrational assignments and electronic structure of these oligomers and of PANI-LB.

3.1. Geometric Structure. The first oligomer studied is diphenyl amine (DPA). In DPA, the bridging nitrogen is connected to two phenyl rings and the effect of steric repulsion arises from the proximity of the phenyl rings. In the present work, we have optimized the two torsional angles Φ(C3−C4−N12−C14) and Φ′(C4−N12−C14−C15) (see Figure 1) independently. It can be seen (Table 1) that our HF/6-31G** basis set calculations reproduce the experiment very well in the case of DPA, including the bond lengths and the bond angle between the two phenyl rings (angle C4−N12−C14 in Figure 1) and clearly show that the torsional angles Φ and Φ′ between the rings have two different values of 15.9 and 46.2°.

As in the HF calculations electron correlation is neglected so when number of atoms increases in the polymeric chain, DFT results appear more close to the experimental values and we can see for PCD molecule from Table 2 (Figure 2) that the DFT calculated bond angle (129.2°) between the phenyl rings is much closer to the experimental value (128.9°) as compared to HF calculated value (125.7°). HF theory is incapable of producing accurate values of backbone torsion angles Φ and Φ′ even with the higher basis set 6-31G** used in the present work, and in our DFT calculations, we found that the two torsional angles Φ and Φ′ are 18.3 and 33.5°, respectively.

Phenyl-end-capped tetramer (B5, $N = 5$) is the next oligomer in the sequence. It serves as a model for the geometry and force field of LB polymer. The B3-LYP optimized structure of B5 is shown in Figure 3, and its geometry is given in Table 3.

TABLE 5: Observed and Calculated Raman and IR Frequencies of PCD (in cm^{-1})[a]

observed			
Raman	IR	calculated frequency	assignments (% PED)
1617		1615	R2[υ(CC)(58) + δ(CHC)(16) + δ(CCC)(10)]
1590		1598	R1[υ(CC) (23)] + R3[υ(CC)(23)]
	1600	1597	R1[υ(CC)(24) + δ(CCC)(5)] + R3[υ(CC)(24) + δ(CCC)(5)]
		1579	R1[υ(CC)(25)] + R3[υ(CC)(25)] + N1[δ(CHN)(7)] + N2[δ(CHN)(7)]
		1577	R1[υ(CC)(32)] + R3[υ(CC)(31)]
		1568	R2[υ(CC)(50) + δ(CCC)(6)]
	1511	1509	R2[δ(CHC)(10)] + υ(CC)(8)] + N1[δ(CHN)(14) + υ(CN)(14)] + N2(δ(CHN)(14) + υ(CN)(14)]
		1493	R2[δ(CHC)(32) + υ(CC)(20)] + N1[δ(CHN)(5)] + N2[δ(CHN)(4)]
		1492	R1[δ(CHC)(11) + υ(CC)(4)] + R3[δ(CHC)(16) + υ(CC)(8)] + N1[δ(CHN)(5) + υ(CN)(7)] + N2[δ(CHN)(6) + υ(NC)(8)]
1497	1494	1487	R1[δ(CHC)(19) + υ(CC)(9)] + R3[δ(CHC)(19) + (υ(CC)(9)] + N1[δ(CHN)(5)] + N2[δ(CHN)(4)]
		1474	R1[δ(CHC)(19) + υ(CC)(8)] + R3[δ(CHC)(21) + υ(CC)(8)] + N1[δ(CHN)(9)] + N2[δ(CHN)(9)]
	1451	1450	R1[δ(CHC)(15) + υ(CC)(12)] + R2[δ(CHC)(6) + υ(CC)(12)] + R3[δ(CHC)(15) + υ(CC)(12)]
1413		1413	R1[δ(CHC)(13) + υ(CC)(11)] + R3[δ(CHC)(13) + υ(CC)(11)] + N1[δ(CHN)(9)] + N2[δ(CHN)(9)]
	1396	1384	R2[δ(CHC)(22) + υ(CC)(34)] + N1[δ(CHN)(7)] + N2[δ(CHN)(7)]
	1335	1323	R1[δ(CHC)(3) + υ(CC)(26)] + R3[δ(CHC)(4) + υ(CC)(26)] + N1[υ(CN)(8)] + N2[υ(CN)(8)]
	1311	1317	R1[δ(CHC)(18) + υ(CC)(28)] + R3[δ(CHC)(17) + υ(CC)(27)]
1309		1310	R1[δ(CHC)(31)] + R3[δ(CHC)(31)] + N1[υ(CN)(5)] + N2[υ(NC)(5)]
		1300	R1[υ(CC)(7)] + R2[υ(CC)(42)] + R3(υ(CC)(7)]
		1296	R1[δ(CHC)(9)] + R2[δ(CCC)(3) + υ(CC)(18)] + R3[δ(CHC)(9)] + N1[υ(CN)(19)] + N2[υ(CN)(8) + υ(NC)(11)]
		1295	R1[υ(CC)(3) + δ(CHC)(43)] + R3[υ(CC)(3)] + N1[υ(NC)(4)] + N2[υ(CN)(4)]
1222		1219	R1[υ(CC)(11)] + R2[δ(CHC)(20)] + R3[υ(CC)(11)] + N1[δ(CHN)(8)] + N2[δ(CHN)(8)]
	1224	1219	R1[υ(CC)(7)] + R2[υ(CC)(30)] + R3[υ(CC)(7)] + N1[δ(CHN)(7) + υ(CN)(4)] + N2[δ(CHN)(7) + υ(NC)(4)]
		1209	R2[δ(CCC)(15) + δ(CHC)(14) + υ(CC)(10)] + N1[υ(CN)(18)] + N2[υ(CN)(17)]
1193		1208	R1[δ(CHC)(27)] + R2[δ(CHC)(24)] + R3[δ(CHC)(26)]
1156	1155	1156	R1[δ(CHC)(10)] + R2[δ(CHC)(54)] + R3[δ(CHC)(10)]
	1137	1140	R1[δ(CHC)(32)] + R3[δ(CHC)(48)] + R3[υ(CC)(6)]
		1140	R1[δ(CHC)(47) + υ(CC)(6)] + R3[δ(CHC)(32)]
		1103	R2[δ(CHC)(62) + υ(CC)(22)]
		1071	R1[δ(CHC)(19) + υ(CC)(23)] + R3[δ(CHC)(19) + υ(CC)(23)]
	1077	1070	R1[δ(CHC)(18) + υ(CC)(23)] + R3[δ(CHC)(17) + υ(CC)(22)]
1028		1016	R1[δ(CHC)(6) + υ(CC)(30)] + R3[δ(CHC)(6) + υ(CC)(31)]
	1025	1015	R1[δ(CHC)(6) + υ(CC)(31) + R3[δ(CHC)(6) + υ(CC)(31)]
		997	R2[δ(CCC)(44) + δ(CHC)(16) + υ(CC)(40)]
993		990	R1[δ(CCC)(34) + υ(CC)(10)] + R3[δ(CCC)(35) + υ(CC)(10)]
	993	990	R1[δ(CCC)(35) + υ(CC)(10)] + R3[δ(CCC)(34) + υ(CC)(10)]
		946	R1[oop(HCCC)(44) + τ(CCCC)(7)] + R3[oop(HCCC)(37) + τ(CCCC)(6)]
		926	R1[oop(HCCC)(40) + τ(CCCC)(3)] + R2[oop(HCCC)(10) + oop(HCCC)(35)]
		926	R1[oop(HCCC)(35)] + R2[oop(HCCC)(8)] + R3[oop(HCCC)(40) + τ(CCCC)(3)]
		914	R1[oop(HCCC)(5)] + R2[oop(HCCC)(70) + τ(CCCC)(6)] + R3[oop(HCCC)(5)]
		912	R1[oop(HCCC)(4)] + R2[oop(HCCC)(66) + τ(CCCC)(14)] + R3[oop(HCCC)(4)]
883		873	R1[δ(CCC)(3) + υ(CC)(3)] + R2[δ(CCC)(5) + υ(CC)(48)] + R3[δ(CCC)(3) + υ(CC)(3)] + N1[υ(NC)(4)] + N2[υ(CN)(4)]
	875	872	R1[oop(HCCC)(37) + τ(CCCC)(3)] + R3[oop(HCCC)(36) + oop(NCCC)(4)] + N2[oop(NCCC)(4)]
843		857	R1[oop(HCCC)(36)] + R3[oop(HCCC)(37) + τ(CCCC)(3)] + N1[oop(NCCC)(4)] + N2[oop(NCCC)(4)]
		855	R1[δ(CCC)(7) + υ(CC)(12)] + R2[δ(CCC)(19)] + R3[δ(CCC)(7) + υ(CC)(12)] + N1[υ(CN)(5)] + N2[υ(NC)(5)]
	819	816	R2[oop(HCCC)(58)] + R2[τ(CCCC)(10)] + N1[oop(NCCC)(8)] + N2[oop(NCCC)(8)]

TABLE 5: Continued

observed			
Raman	IR	calculated frequency	assignments (% PED)
820		814	R1[oop(HCCC)(8) + υ(CC)(3)] + R2[oop(HCCC)(10) + τ(CCCC)(5)] + R3[oop(HCCC)(8) + υ(CC)(3)] + N1[δ(CCN)(5)] + N2[δ(CCN)(5)
		802	R1[oop(HCCC)(51)] + R2[oop(HCCC)(12)]
		802	R1[oop(HCCC)(13)] + R3[oop(HCCC) (64)]
	771	770	R1[oop(HCCC)(11)] + R2[oop(HCCC)(70)] + R3[oop(HCCC)(11)]
757	746	759	R1[oop(HCCC)(3) + τ(CCCC)(5)] + R2[δ(CCC)(7) + oop(HCCC)(10)] + R3[oop(HCCC)(3) + τ(CCCC)(5)] + N1[δ(CCN)(7) + oop(NCCC)(5)] + N2[δ(CCN)(7) + oop(NCCC)(5)]
		746	R1[oop(HCCC)(22) + τ(CCCC)(12)] + R3[oop(HCCC)(22) + τ(CCCC)(12)] + N1[oop(NCCC)(8)] + N2[oop(NCCC)(8)]
		728	R1[oop(HCCC)(28) + τ(CCCC)(9)] + R3[oop(HCCC)(28) + τ(CCCC)(9)] + N1[oop(NCCC)(6)] + N2[oop(NCCC)(6)]
722		699	R2[τ(CCCC)(57)] + N1[oop(NCCC)(13)] + N2[oop(NCCC)(13)]
		690	R1[oop(HCCC)(11) + τ(CCCC)(31)] + R2[τ(CCCC)(3)] + R3[oop(HCCC)(11) + τ(CCCC)(31)] + N1[oop(NCCC)(5)] + N2[oop(NCCC)(5)]
	694	678	R1[oop(HCCC)(11) + τ(CCCC)(33)] + R3[oop(HCCC)(11) + τ(CCCC)(33)]
661		649	R1[δ(CCC)(7)] + R2[δ(CCC)(28) + τ(CCCC)(9)] + R3[δ(CCC)(7)] + N1[δ(CNC)(7)] + N2[δ(CNC)(7)]
622		613	R1[δ(CCC)(22)] + R2[δ(CCC)(27) + τ(CCCC)(8)] + R3[δ(CCC)(22)]
	610	606	R1[δ(CCC)(42)] + R3[δ(CCC)(42)]
		600	R1[δ(CCC)(14)] + R2[δ(CCC)(25) + τ(CCCC)(14)] + R3[δ(CCC)(14)] + N1[δ(CCN)(7)] + N2[δ(CCN)(7)]
		599	R1[δ(CCC)(24) + R3[δ(CCC)(24)] + N1[δ(CCN)(8) + oop(NCCC)(3)] + N2[δ(CCN)(8) + oop(NCCC)(3)]
556		546	R1[δ(CCC)(24)] + R2[δ(CCC)(34)] + R3[δ(CCC)(24)]
508	514	510	R2[τ(CCCC)(27)] + N1[oop(NCCC)(27)] + N2[oop(NCCC)(27)]
		491	R1[oop(HCCC)(5) + τ(CCCC)(21)] + R3[oop(HCCC)(5) + τ(CCCC)(22)] + N1[oop(NCCC)(18)] + N2[oop(NCCC)(19)]
		489	R1[oop(HCCC)(4) + τ(CCCC)(17)] + R2[τ(CCCC)(5)] + R3[oop(HCCC)(4) + τ(CCCC)(17)] + N1[oop(NCCC)(16)] + N2[oop(NCCC)(15)]
	405	409	R1[τ(CCCC)(14)] + R2[oop(HCCC)(8) + τ(CCCC)(49)] + R3[τ(CCCC)(14)]
418		405	R1[τ(CCCC)(40)] + R3[τ(CCCC)(40)]
		402	R1[τ(CCCC)(25)] + R2[τ(CCCC)(31)] + R3[τ(CCCC)(25)]
407		393	R2[δ(CCC)(8) + τ(CCCC)(11)] + N1[δ(CNC)(20) + oop(NCCC)(8)] + N2[δ(CNC)(20) + oop(NCCC)(8)]
		358	R1[δ(CCC)(7)] + R3[δ(CCC)(7)] + N1[δ(CCN)(5) + δ(CNC)(14) + (υ(CN)(10)] + N2[δ(CCN)(5) + δ(CNC)(14) + υ(CN)(10)]
328		329	N1[oop(HCCN)(9) + τ(CCNH)(19) + τ(CNCC)(19)] + N2[oop(HCCN)(9) + τ(CCNH)(18) + τ(CNCC)(18)]
		309	R2[τ(CCCC)(17) + δ(CNC)(19)] + N1[oop(NCCC)(10)] + N2[δ(CNC)(19) + oop(NCCC)(10)]
		307	N1[oop(HCCN)(9) + τ(CCNH)(15) + τ(CNCC)(15)] + N2[oop(HCCN)(10) + τ(CCNH)(16) + τ(CNCC)(16)]
		292	R1[τ(CCCC)(6)] + R3[τ(CCCC)(6)] + N1[δ(CNC)(18) + τ(CCNH)(8) + τ(CNCC)(7)] + N2[δ(CNC)(18) + τ(CCNH)(8) + τ(CNCC)(8)]
260		243	R1[τ(CCCC)(11)] + R2[δ(CCC)(16)] + R3[τ(CCCC)(11)] + N1[δ(CNC)(8)] + N2[δ(CNC)(8)]
226		207	R1[τ(CCCC)(24)] + R2[δ(CCC)(7)] + R3[τ(CCCC)(24)]
		190	R1[τ(CCCC)(27)] + R3[τ(CCCC)(27)] + N1[δ(CNC)(4) + oop(NCCC)(4)] + N2[δ(CNC)(4) + oop(NCCC)(4)]
		164	R2[oop(HCCC)(8) + τ(CCCC)(37) + N1[δ(CCN)(5) + δ(CNC)(4) + τ(CCNH)(4)] + N2[δ(CCN)(5) + δ(CNC)(4) + τ(CNCC)(4)
		109	R1[τ(CCCC)(10)] + R3[τ(CCCC)(10)] + N1[δ(CCN)(9) + oop(NCCC)(3) + τ(CCNH)(4) + τ(CNCC)(11)] + N2[δ(CCN)(9) + oop(NCCC)(4) + τ(CCNH)(11) + τ(CNCC)(4)]
		57	N1[δ(CCN)(16) + δ(CNC)(9) + τ(CCNH)(8) + τ(CNCC)(15)] + N2[δ(CCN)(16) + δ(CNC)(9) + τ(CCNH)(15) + τ(CNCC)(8)]
		50	R2[τ(CCCC)(40)] + N1[τ(CNCC)(18)] + N2[τ(CCNH)(17)]
		36	N1[δ(CCN)(14) + δ(CNC)(11) + τ(CCNH)(15) + τ(CNCC)(5) + [N2(δ(CCN)(14) + δ(CNC)(11) + τ(CCNH)(5) + τ(CNCC)(15)]
		33	N1[oop(HCCN)(19) + τ(CCNH)(15) + τ(CNCC)(11)] + N2[oop(HCCN)(19) + τ(CCNH)(11) + τ(CNCC)(14)]
		15	N1[τ(CNCC)(18) + τ(CCNH)(13)] + N2[oop(HCCN)(13) + τ(CCNH)(17) + τ(CNCC)(12)]

[a] Note: All frequencies are in cm^{-1}. R1, R2, and R3 are the three benzoid rings, and N1, N2, and N3 are the three nitrogen atoms in the molecular structure of PCD. υ, δ, and τ are the symbols used for stretch, bend, and torsional motions.

Although no experimental data are available for the geometry of B5, the DFT optimized geometry appears to be more accurate, as its HF and DFT calculated geometry results are on the same sequence as that of PCD's HF and DFT calculated results.

3.2. Vibrational Analysis. ***Raman Spectra of Leucoemeraldine Base and Its Oligomers.*** *DPA.* The molecular structure of DPA is shown in Figure 1. A comparison of the observed[32,35] and calculated scaled Raman spectra of DPA is shown in parts a and b of Figure 4 for the regions 1650−850 and 850−200 cm^{-1}, respectively. Assignments of different bands with their PED are given in Table 4. Raman spectra in the frequency range 1650−850 cm^{-1} are mainly composed of seven bands peaked at 1603, 1589, 1220, 1183, 1153, 1031, and 993 cm^{-1}. The most intense peak at 1603 cm^{-1} is assigned to the calculated band at 1604 cm^{-1} and is found to be associated with CC stretch of the two phenyl rings and corresponds to the 8(a) vibrational mode of the monosubstituted benzenes. The next band in the Raman spectra is a shoulder at 1586 cm^{-1}; in our calculated spectra, we found an exactly similar band at 1592 cm^{-1} having the nature of CC stretching 8(a). Weak bands at 1493, 1340, and 1306 cm^{-1} are representative of 19b, 3, and 14 CH in-plane bending vibrations. The strong peak at 1220 cm^{-1} is assigned to the

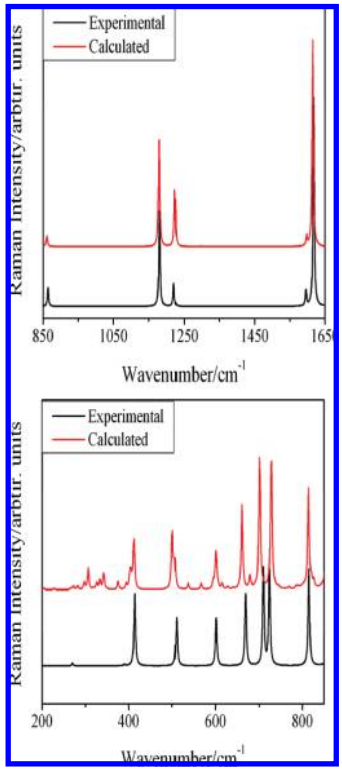

Figure 6. (a) Experimental[32] and calculated Raman spectra of PANI-LB (850−1650 cm^{-1}). (b) Experimental[35] and calculated Raman spectra of PANI-LB (200−850 cm^{-1}).

calculated band at 1208 cm^{-1} which is a mixed mode having CN and CC stretching vibrations (vibration 13). The two bands at 1183 and 1157 cm^{-1} are found to be associated with C−H in-plane bending vibrations 9a and 15, respectively, of the phenyl rings. The next prominent peak in the observed Raman spectra at 1031 cm^{-1} is assigned to a similar calculated peak at 1017 cm^{-1} which is a mixed mode of CHC bend and CC stretching corresponding to the 18a vibration of the monosubstituted benzenes. CCC bending (breathing) and CC stretching vibrations are generally found to be mixed in monosubstituted benzenes, and we found the observed band in this region at 993 cm^{-1} to be associated with CCC bending and CC stretching. In the lower region of the spectra below 900 cm^{-1}, we have numerous weak peaks; among them, the peaks at 878, 837, 818, and 752 are due to the CH wagging motion of the rings and can be seen as 17b, 10a, and 11 Wilson vibrations. The bands at 641, 616, and 568 cm^{-1} are assigned to the calculated mode at 629, 608, and 559 cm^{-1}, respectively, and can be regarded as 1, 6b, and 6a radial skeletal vibrations having a main contribution of CCC bend in their PED. The bands at 507 cm^{-1} is related to torsional motion of the two rings mixed with CN out-of-plane vibrations, while the bands at 415 and 221 cm^{-1} are related to only torsional motion of rings (16a and 16b Wilson vibrations). The intense band at 308 cm^{-1} is assigned to in-plane rotation of the rings mixed with CN in-plane bend and CN stretch.

PCD. A comparison of the observed[32,35] and calculated scaled Raman spectra of PCD is shown in parts a and b of Figure 5 for the regions 1650−850 and 850−200 cm^{-1}, respectively. Assignments of different bands with their PED are given in Table 5. The most intense band in the Raman spectra of PCD is at 1617 cm^{-1}, which is the characteristic of the central benzene ring (disubstituted in para position) having CC stretching vibrations. A weak shoulder at 1590 cm^{-1} is assigned to the calculated band at 1598 cm^{-1} having CC stretching of the two monosubstituted benzenes. Similar to the DPA bands at 1183 and 1157 cm^{-1}, in PCD, we can observe bands at 1192 and 1156 cm^{-1} which are CH in-plane bending vibrational modes of the phenyl rings. The bands at 1031 and 993 cm^{-1} in DPA are found at 1028 and 993 cm^{-1} in the PCD and are due to the CH in-plane bending and CCC bending vibrations, respectively. In the spectra below 850 cm^{-1} (Figure 5b), the bands at 843 and 820 cm^{-1} are due to the out-of-plane CH vibrations. The intense bands at 722 and 661 cm^{-1} are assigned to calculated modes at 699 and 649 cm^{-1}, respectively, in which the first one is due to out-of-plane ring deformation of the central ring and the second is due to out-of-plane deformation of all three rings. The bands at 622 and 556 cm^{-1} are assigned to an in-plane deformation of the rings, while the bands at 418 and 226 cm^{-1} are also due to the out-of plane deformations of the ring.

PANI-LB. Phenyl-end-capped tetramer (B5) is used as a model oligomer for the vibrational analysis of the LB polymer. A comparison of the observed[32,35] and calculated Raman spectra of PANI-LB is presented in Figure 6, and assignments of all of the bands with their PED are given in Table 6. The spectrum exhibits several characteristic bands of the benzene ring such as those peaked at 1618 and 1181 cm^{-1} (1603 and 1183 cm^{-1} in DPA, 1618 and 1182 cm^{-1} in PCD) that correspond to a CC stretching vibration and a CH bending vibration, respectively. The band at 1618 and a distinct shoulder at 1597 cm^{-1} are assigned to the calculated bands at 1615 and 1598 cm^{-1}, respectively, which mainly involve "quadrant stretching" of the ring CC bonds with a partial contribution of the in-plane CH bending (vibrational modes 8a and 8b). The band at 1219 cm^{-1} in LB (1220 cm^{-1} in DPA, 1222 cm^{-1} in PCD) is related to the symmetric C−N stretching vibrations. One of the most intense bands in the Raman spectra of all oligomers studied is the band observed at about 1180 cm^{-1} (1183 in DPA and 1177 cm^{-1} in PCD), and as the number of aromatic rings increases, its intensity increases. In PANI-LB, it appears as an intense line at 1181 cm^{-1}; this line can be regarded as a pure CH in-plane bending vibration and corresponds to the 9a vibrational mode. The intensity of the contributions due to the outer rings decreases (the two bands at 993 and 1031 cm^{-1} in DPA are found weaker in PCD and are not observed in the polymer) when the chain length increases, which is consistent with the polymeric nature of the compound studied and confirms our assignments. Below 900 cm^{-1}, we have bands at 864 and 816 cm^{-1} which are associated with CH wagging 10a and 11 Wilson vibrations. Bands at 724 and 710 cm^{-1} are due to the out-of-plane skeletal vibrations (Wilson vibration 4). The peak at 669 cm^{-1} is assigned to the CC in-plane ring deformation. The 16a and 16b Wilson vibrations of para-disubstituted benzenes are the vibrations having out-of-plane skeletal vibration, and in the Raman spectra of PANI-LB, these vibrations are found at 510 and 414 cm^{-1}.

Infrared Spectra of Leucoemeraldine Base and Its Oligomers. *DPA.* A comparison of the observed[32,35] and calculated IR spectra of DPA is presented in Figure 7a and b for the regions 1650−1050 and 1050−400 cm^{-1}, respectively. Assignments of different bands with their PED are given in Table 4. The broad intense band at 1596 cm^{-1} is assigned to the mode calculated at 1592 cm^{-1} and is due to the CC stretching vibration of the benzene ring (8a). The group of bands in the region 1540−1450 cm^{-1} is related to mixed CC stretching and CH and NH bending vibrations. The band at 1417 cm^{-1} is assigned to a mixed mode at 1403 cm^{-1} having CH and NH bend as a major component in their PED. The next intense bands in the IR spectra of DPA

TABLE 6: Observed and Calculated Raman and Infrared Active Frequencies of LB (in cm^{-1})[a]

exptl freq Raman	exptl freq IR	calcd freq	assignments
1618		1615	CC stretch (*8a*)
		1612	CC stretch + CH bending (*8a*)
1597		1598	CC stretch + CH bending (*8b*)
	1596	1598	CC stretch + CH bending (*8b*)
		1508	CC stretch + CH bending (*19a*)
	1496	1508	CC stretch + CH bending + C−H−N bend (*19a*)
		1479	CH bending + CC stretch (*19b*)
		1475	CH bending + CC stretch (*19b*)
		1423	NH bending
		1387	CC stretch + CH bending (*14*)
		1321	CC stretch + CH bending (*14*)
		1311	CH bending (*3*)
		1296	CH bending (*3*)
	1282	1289	CN stretch + CC stretch + C−H bend
1221		1224	CC stretch
	1218	1213	CC stretch + CN stretch (*13*)
		1209	CN stretch (*13*)
		1208	CN stretch (*7a*)
		1206	CN stretch (*7a*)
1181		1180	CH bending (*9a*)
	1167	1163	CH bending (*9a*)
	1107	1110	CH bending (*18b*)
	1009	1006	CH bending + CC stretch (*18a*)
		987	Ring def. i.p.
		987	Ring def. i.p.
		970	Ring def. i.p.
		970	Ring def. i.p.
		946	CH wag (*17a*)
	932	945	CH wag (*17a*)
		924	CH wag (*10b*)
		923	CH wag (*10b*)
868	858	857	CH wag (*10a*)
		826	C H wag (*10a*)
820		821	C H wag (*11*)
		820	C−C−C bend + C−H bend o.p. (*1*)
		815	C H wag (*11*)
	812	814	C−H bend o.p. (*11*)
725		730	C−H bend o.p. + CCC bend o.p. (*4*)
		728	C−H bend o.p. + CC ring def. o.p. + CN bend o.p. (*4*)
	700	701	C−C ring def. o.p. (*4*)
667		661	C−C ring def. i.p. (*6b*)
	621	627	C−C ring def. i.p. (*6b*)
603		601	C−C ring def. i.p. + CN bend i.p.
511	513	506	CN bend o.p. + CC bend o.p (*16b*)
		491	CC torsion + CN bend o.p.
414		409	CC torsion (*16a*)
		334	CN bend o.p. + CC bend o.p.
		326	CN bend o.p.
		306	CNC bending i.p. (*15*)
		297	NH wag + CN bend o.p.
		282	NH wag + CN bend o.p.
		273	CN bend o.p.
		267	CN bend o.p.
		230	CNC bending i.p.

[a] Note: The numbers in italics in parentheses are benzene Wilson numbers. def, deformation; i.p., in-plane; o.p., out-of-plane.

are at 1336 and 1318 cm^{-1}, which are associated with CH in-plane bending vibrations and can be regarded as Wilson vibration 3 of monosubstituted benzenes. The two weak bands at 1172 and 1151 cm^{-1} are due to the CH in-plane bending vibrations and correspond to the 9a and 15 vibrational modes, respectively. In the spectral region below 1050 cm^{-1} (Figure 7b), bands at 1022 cm^{-1} can be seen as 18a Wilson vibration having CC stretch and CC bending vibrations. The strong bands at 846 and 743 cm^{-1} are due to the out-of-plane CH wagging motion, while the band at 686 cm^{-1} is related to out-of-plane CC vibrations and can be seen as normal vibration 4 of monosubstituted benzenes. The band at 641 cm^{-1} is assigned to the in-plane amine deformation mixed with in-plane ring deformation, and the band at 613 cm^{-1} is assigned to the in-plane deformation of the two benzoid rings. Observed bands in the IR spectra at 505 and 428 cm^{-1} are mainly due to out-of-plane CNC torsion and CCC torsion, respectively.

PCD. The calculated IR spectra of PCD together with the observed spectra are presented in Figure 8, and the assignments of different bands are given in Table 5. Similar bands are seen in the IR spectrum of PCD as in the DPA. We observe a band at 1600 cm^{-1} narrower than in DPA, which is due to the CC stretching vibrations of the terminal rings. There is a group of bands around 1500 cm^{-1} in which the intense band at 1511

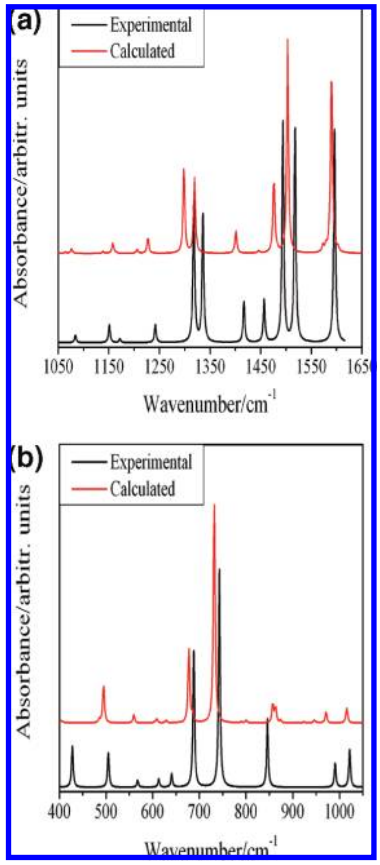

Figure 7. (a) Experimental[32] and calculated IR spectra of DPA (1050−1650 cm^{-1}). (b) Experimental[35] and calculated IR spectra of DPA (400−1050 cm^{-1}).

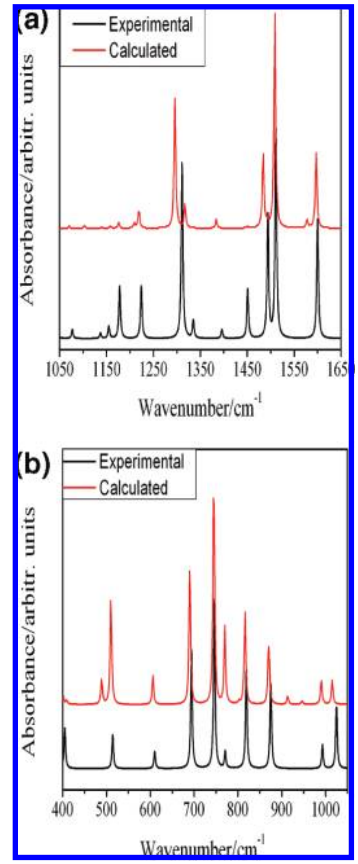

Figure 8. (a) Experimental[32] and calculated IR spectra of PCD (1050−1650 cm^{-1}). (b) Experimental[35] and calculated IR spectra of PCD (400−1050 cm^{-1}).

cm^{-1} is a mixed band of NH rocking, CH bend, and C−N stretch while the band at 1494 cm^{-1} is due to the in-plane CH bending vibration of the terminal rings. The C−H in-plane bending band at 1318 cm^{-1} in DPA is shifted to 1312, 1172 to 1177 cm^{-1}, and 1151 to 1155 cm^{-1} in the PCD. The band at 1223 cm^{-1} is assigned to the CN stretching vibrations. The band at 1025 cm^{-1} is found to be associated with CC stretching and CHC in-plane bending vibrations, while the band at 993 cm^{-1} is with CCC in-plane bending mixed with CC stretch. The bands at 875, 819, and 771 cm^{-1} are associated with the CH wagging motion of the rings. The strong band at 746 cm^{-1} is a completely mixed mode of CH, CN, and CC bending vibrations. Similar to the band at 688 cm^{-1} in DPA, we have a band at 694 cm^{-1}, which is assigned to the out-of-plane CC and CH vibrations. The band at 613 cm^{-1} in DPA appears at 610 cm^{-1} in PCD and is similarly associated with in-plane deformation of the terminal rings. Similar to DPA, the bands in the region 750−700 cm^{-1} are due to out-of-plane vibrations. The band at 514 cm^{-1} is due to the out-of-plane CN and CC bends, and the band at 405 cm^{-1} is due to the out-of-plane CC bend.

PANI-LB. The IR spectrum of the polymer (Figures 9) exhibits far fewer bands than those of the two other compounds. It exhibits mainly three strong bands at 1496, 1282, and 1218 cm^{-1}. Similar to DPA (1596 cm^{-1}) and PCD (1600 cm^{-1}), we can find a band at 1596 cm^{-1} in PANI-LB, which is comparatively very weak and is assigned to CC stretching vibration of the phenyl rings. The most intense band in the spectra at 1496 cm^{-1} is due to the CC stretching and CH in-plane bending of the rings (19a) in the IR spectrum of PANI-LB and its oligomers. We can notice the presence of a vary intense band around 1300 cm^{-1}, which shifts toward lower frequencies when the chain length increases and is located at 1282 cm^{-1} in the PANI-LB. This band is assigned to CN stretching vibration. The out-of-plane CH wag motions are very suitable for the determination of the type of ring substitution in benzene derivatives. In the monosubstituted ring, the out-of-plane ring deformation no. 4 occurs at 688 cm^{-1} in DPA, whereas para-substitution is characterized by an IR absorption band at 819 cm^{-1}. This band involves the out-of-plane deformation vibration 1, where all hydrogens move in-phase and thus give rise to a large dipole moment change and a strong IR band. In LB polymer, we observe only the band at 812 cm^{-1}, while the bands at 750 and 693 cm^{-1} disappear. The strong band at 513 cm^{-1} is found to be associated with CN and CC out-of-plane bending motion. To summarize, we can note that the bands corresponding to the para-disubstituted aromatic ring gain in intensity upon the chain length elongation, whereas the intensity of the bands due to the monosubstituted ring decreases. This observation strongly corroborates our assignment.

C. Electronic Properties of Leucoemeraldine Base. The energy gap between the valence and conduction bands of the polymer is related to the lowest allowed energy of its monomer units and to the bandwidth resulting from the overlap between the monomer orbitals.

The DFT method had successfully been used to study band gaps of conjugated organic polymers where the HOMO/LUMO difference provides a good estimate of the excitation energy. While there is some controversy surrounding the interpretation of DFT orbital energies, we find that the HOMO/LUMO energy difference offers a very good estimate of band gaps. It should be noted that the HOMO/LUMO energy difference at *ab initio* levels does not closely relate to excitation energies due to the

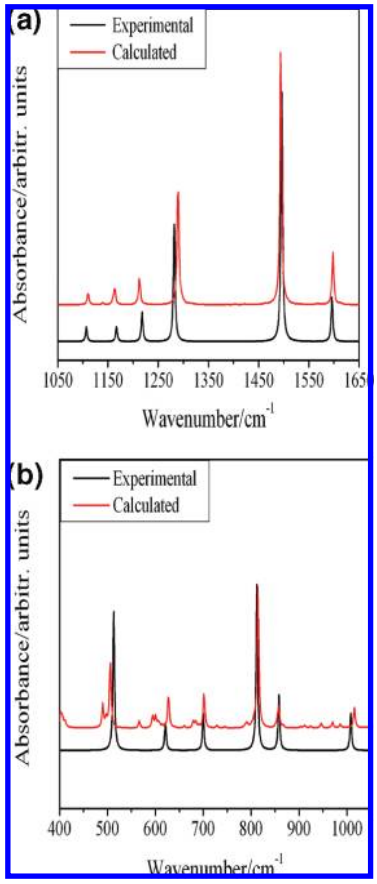

Figure 9. (a) Experimental[32] and calculated IR spectra of PANI-LB (1050−1650 cm^{-1}). (b) Experimental[35] and calculated IR spectra of PANI-LB (400−1050 cm^{-1}).

TABLE 7: Calculated and Experimental Values of the Band Gap of DPA, PCD, and LB in eV

molecule	calculated	band gap, experimental[a]	earlier calculated work[b]
DPA	4.95		
PCD	4.42		
LB	4.01	3.8−4.0	4.29

[a] Reference 66. [b] Reference 33.

absence of orbital relaxation effects. Values of the band gap of LB and its oligomers along with experimental values are given in Table 7, and we found that the DFT calculated band gap value (4.01 eV) of LB is much closer to the experimental observed values (3.8−4.0 eV)[66] as compared to the earlier calculated values.[33]

4. Conclusion

We have carried out quantum chemical calculations at both *ab initio* and DFT levels of a series of oligomers of an important member of the polyaniline family, leucoemeraldine base. Geometry optimizations of the oligomers are followed by complete vibrational analysis using the 6-31G** basis set. DFT methods have given rise to better prediction of the structural parameter as compared to *ab initio* methods. With the help of the B3LYP/6-31G** method we find that the total torsional angle between the different phenyl rings (the sum of angle Φ and Φ′) is around 52° in the LB chain. DFT calculation with this higher basis set gives us a very good match between the observed and calculated IR and Raman spectra. Assignments of all of the bands are being presented keeping in mind the PED calculations, band shape, and standard Wilson vibrations of mono- and para-disubstituted benzenes. The DFT calculated value of the band gap of PANI-LB is very close to the experimental value, which also confirms our assignments.

References and Notes

(1) Chiang, C. K.; Fincher, C. R., Jr.; Park, Y. W.; Hegger, A. J.; Shirakawa, H.; Louis, E. J.; Gau, S. C.; MacDiarmid, A. G. *Phys. Rev. Lett.* **1977**, *39*, 1098.
(2) Nalwa, H. S. *Handbook of Organic Conducting Molecules and Polymers*; Wiley: Chichester, U.K., 1997; Vols. I−IV.
(3) Ray, A.; Asturias, G. E.; Kershner, D. L.; Richter, A. F.; MacDiarmid, A. G.; Epstein, A. J. *Synth. Met.* **1989**, 29.
(4) Neoh, K. G.; Kang, E. T.; Khor, S. H.; Tan, K. L. *Polym. Degrad. Stab.* **1990**, *27*, 107.
(5) Tan, K. L.; Tan, B. T. G.; Kang, E. T.; Neoh, K. G. *J. Chem. Phys.* **1991**, *94*, 5382.
(6) Letheby, H. *J. Chem. Soc.* **1862**, *15*, 161.
(7) de Surville, R.; Jozefowicz, M.; Yu, L. T.; Perichon, J.; Buvet, R. *Electrochim. Acta* **1968**, *13*, 1451.
(8) Diaz, A. F.; Logan, J. A. *J. Electroanal. Chem.* **1980**, *111*, 111.
(9) Kobayashi, T.; Yoneyama, H.; Tamura, H. *J. Electroanal. Chem.* **1984**, *177*, 281.
(10) Genies, E. M.; Tsintavis, C. *J. Electroanal. Chem.* **1984**, *195*, 109.
(11) Macdiarmid, A. G.; Mu, S. L.; Somasiri, N. L. D.; Wu, W. *Mol. Cryst. Liq. Cryst.* **1985**, *121*, 181.
(12) Genies, E. M.; Syed, A. A.; Tsintavis, C. *Mol. Cryst. Liq. Cryst.* **1985**, *121*, 187.
(13) Salaneck, W. R.; Lundstrom, I.; Liedberg, B.; Hasan, M. A.; Erlandsson, R.; Konradsson, P.; Macdiarmid, A. G.; Somasiri, N. L. D. *Solid State Sci.* **1985**, *63*, 218.
(14) Schacklette, L. W.; Maxfield, M.; Gould, S.; Wolf, J. F.; Jow, T. R.; Baughman, R. H. *Synth. Met.* **1987**, *18*, 611.
(15) Okabayashi, K.; Goto, F.; Abe, K.; Yoshida, T. *Synth. Met.* **1987**, *18*, 365.
(16) Macdiarmid, A. G.; Yang, L. S.; Haung, W. S.; Humphrey, B. D. *Synth. Met.* **1987**, *18*, 611.
(17) Genies, E. M.; Hany, P.; Santier, Ch. *J. Appl. Electrochem.* **1988**, *18*, 751.
(18) Wang, B.; Li, G.; Li, C.; Wang, F. *J. Power Sources* **1988**, *24*, 115.
(19) Paul, E. W.; Ricco, A. J.; Wrighton, M. S. *J. Phys. Chem.* **1985**, *89*, 1441.
(20) Boyle, A.; Genies, E. M.; Lapkowski, M. Proceedings of ICSM '88, Santa Fe/USA, Synth Metals 1989;63:211.
(21) Kobayashi, T.; Yoneyama, H.; Tamura, H. *J. Electroanal. Chem.* **1984**, *161*, 419.
(22) Kitani, A.; Yano, J.; Sasaki, K. *J. Electroanal. Chem.* **1986**, *209*, 227.
(23) Aurian-Blajeni, B.; Taniguchi, I.; Bochris, J. O. M. *J. Electroanal. Chem.* **1983**, *149*, 291.
(24) Green, A. G.; Woodhead, A. E. *J. Chem. Soc. Trans* **1910**, *97*, 2388.
(25) Green, A. G.; Woodhead, A. E. *J. Chem. Soc. Trans.* **1912**, *101*, 1117.
(26) Ray, A.; Asturias, G. E.; Kershner, D. L.; Richter, A. F.; Macdiarmid, A. G.; Epstein, J. *Synth. Met.* **1989**, *29*, E141.
(27) Ray, A.; Richter, A. F.; Macdiarmid, A. G.; Epstein, A. J. *Synth. Met.* **1989**, *29*, E151.
(28) Zerbi, G.; Gussoni, M.; Castiglioni, C. In *Conjugated Polymers*; Bredas, J. L., Silbey, R., Eds.; Kluwer Academic Publishers: Dordrecht, The Netherlands, 1991; p 435.
(29) Gussoni, M.; Castiglioni, C.; Zerbi, G. In *Spectroscopy of Advanced Materials*; Clark, R. J. H., Hester, R. E., Eds.; John Wiley and Sons: Chichester, England, 1991; p 251.
(30) Quillard, S.; Louarn, G.; Buisson, J. P.; Lefrant, S.; Masters, J.; MacDiarmid, A. G. *Synth. Met.* **1992**, *49−50*, 525.
(31) Quillard, S.; Louarn, G.; Buisson, J. P.; Lefrant, S.; Masters, J.; MacDiarmid, A. G. *Synth. Met.* **1993**, *55−57*, 475.
(32) Quillard, S.; Louarn, G.; Lefrant, S.; Masters, J.; MacDiarmid, A. G. *Phys. Rev.* **1994**, *50*, 12496.
(33) Choi, C. H.; Kertesz, M. *Macromolecules* **1997**, *30*, 620.
(34) Boyer, M. I.; Quillard, S.; Rebourt, E.; Louarn, G.; Buisson, J. P.; Monkman, A.; Lefrant, S. *J. Phys. Chem. B* **1998**, *102*, 7382.
(35) Cochet, M.; Louarn, G.; Quillard, S.; Boyer, M. I.; Buisson, J. P.; Lefrant, S. *J. Raman Spectrosc.* **2000**, *31*, 1029.
(36) Mishra, A. K.; Tandon, P.; Gupta, V. D. *Macromol. Symp.* **2008**, *265*, 111.
(37) Suhai, S. *Phys. Rev. B* **1994**, *50*, 14791.
(38) Bartlett, R. J. *Annu. Rev. Phys. Chem.* **1981**, *32*, 359.

(39) Bartlett, R. J. *J. Phys. Chem.* **1989**, *93*, 1697.
(40) Raghavachari, K.; Trucks, G. W.; Pople, J. A.; Head-Gordon, M. *Chem. Phys. Lett.* **1989**, *157*, 479.
(41) Del Bene, J. E.; Person, W. B.; Szczepaniak, K. *J. Phys. Chem.* **1995**, *99*, 10705.
(42) Gutsev, G. L.; Bartlett, R. J. *Chem. Phys. Lett.* **1997**, *265*, 12.
(43) Bureau, C.; Chong, D. P.; Lecayon, G.; Delhalle, J. *J. Electron Spectrosc. Relat. Phenom.* **1997**, *83*, 227.
(44) Oliphant, N.; Bartlett, R. J. *J. Chem. Phys.* **1994**, *100*, 6550.
(45) Suhai, S. *J. Phys. Chem.* **1995**, *99*, 1172.
(46) Sun, J. Q.; Bartlett, R. J. *Phys. Rev. Lett.* **1996**, *77*, 3669.
(47) Miao, M. S.; Van Camp, P. E.; Van Doren, V. E.; Ladik, J. J.; Mintmire, J. W. *Phys. Rev. B* **1996**, *54*, 10430.
(48) Champagne, B.; Perpete, E. A.; Van Gisbergen, S. J. A.; Baerends, E. J.; Snijders, J. G.; Soubra-Ghaoui, C.; Robins, K. A.; Kirtman, B. *J. Chem. Phys.* **1998**, *109*, 10489.
(49) Mishra, A. K.; Tandon, P. *J. Phys. Chem. B* **2009**, *113* (29), 9702.
(50) Suhai, S. *Phys. Rev. B* **1995**, *51*, 16553.
(51) Honda, K.; Furukawa, Y.; Nishide, H. *Vib. Spectrosc.* **2006**, *40*, 149.
(52) Murakami, R.; Sato, H.; Dybal, J.; Iwata, T.; Ozaki, Y. *Polymer* **2007**, *48*, 2672.
(53) Ramer, N. J.; Marrone, T.; Stiso, K. A. *Polymer* **2006**, *47*, 7160.
(54) Frisch, M. J.; Trucks, G. W.; Schlegel, H. B.; Scuseria, G. E.; Robb, M. A.; Cheeseman, J. R.; Montgomery, J. A., Jr.; Vreven, T.; Kudin, K. N.; Burant, J. C.; Millam, J. M.; Iyengar, S. S.; Tomasi, J.; Barone, V.; Mennucci, B.; Cossi, M.; Scalmani, G.; Rega, N.; Petersson, G. A.; Nakatsuji, H.; Hada, M.; Ehara, M.; Toyota, K.; Fukuda, R.; Hasegawa, J.; Ishida, M.; Nakajima, T.; Honda, Y.; Kitao, O.; Nakai, H.; Klene, M.; Li, X.; Knox, J. E.; Hratchian, H. P.; Cross, J. B.; Bakken, V.; Adamo, C.; Jaramillo, J.; Gomperts, R.; Stratmann, R. E.; Yazyev, O.; Austin, A. J.; Cammi, R.; Pomelli, C.; Ochterski, J. W.; Ayala, P. Y.; Morokuma, K.; Voth, G. A.; Salvador, P.; Dannenberg, J. J.; Zakrzewski, V. G.; Dapprich, S.; Daniels, A. D.; Strain, M. C.; Farkas, O.; Malick, D. K.; Rabuck, A. D.; Raghavachari, K.; Foresman, J. B.; Ortiz, J. V.; Cui, Q.; Baboul, A. G.; Clifford, S.; Cioslowski, J.; Stefanov, B. B.; Liu, G.; Liashenko, A.; Piskorz, P.; Komaromi, I.; Martin, R. L.; Fox, D. J.; Keith, T.; Al-Laham, M. A.; Peng, C. Y.; Nanayakkara, A.; Challacombe, M.; Gill, P. M. W.; Johnson, B.; Chen, W.; Wong, M. W.; Gonzalez, C.; Pople, J. A. Gaussian 03, revision C.02; Gaussian, Inc.: Wallingford, CT, 2003.
(55) Computer Program GaussView, Ver. 2; Gaussian, Inc.: Pittsburgh, PA.
(56) Zhurko, G. A.; Zhurko, D. A. ChemCraft: tool for treatment of chemical data, lite version build 08 (freeware); 2005.
(57) Becke, A. D. *Phys. Rev. A* **1988**, *38*, 3098.
(58) Lee, C.; Yang, W.; Parr, R. G. *Phys. Rev. B* **1988**, *37*, 785.
(59) Pulay, P.; Fogarasi, G.; Pang, F.; Boggs, J. E. *J. Am. Chem. Soc.* **1979**, *101*, 2550.
(60) Fogarasi, G.; Zhou, X.; Taylor, P. W.; Pulay, P. *J. Am. Chem. Soc.* **1992**, *114*, 8191.
(61) Teramae, H.; Yamabe, T.; Imamura, A. *J. Chem. Phys.* **1984**, *81*, 3564.
(62) Kofranek, M.; Lischka, H.; Karpfen, A. *J. Chem. Phys.* **1992**, *96*, 982.
(63) Wong, M. W. *Chem. Phys. Lett.* **1996**, *256*, 391.
(64) Scott, A. P.; Radom, L. *J. Phys. Chem.* **1996**, *100*, 16502.
(65) Martin, J. M. L.; Van Alsenoy, C. 1995. Gar2ped. University of Antwerp, 1995.
(66) McCall, R. P.; Ginder, J. M.; Leng, J. M.; Ye, H. J.; Manoher, S. K.; Masters, J. G.; Asturias, G. E.; MacDiarmid, A. G.; Epsein, A. J. *Phys. Rev. B* **1990**, *41*, 5202.

JP906799M